Space-Qualified Superconductive Digital Instantaneous Frequency-Measurement Subsystem

Guo-Chun Liang, *Senior Member, IEEE,* Chien-Fu Shih, Richard S. Withers, *Member, IEEE,* Brady F. Cole, and Marie E. Johansson

(Invited Paper)

Abstract— **We have constructed a five-bit high temperature superconductive digital instantaneous frequency measurement (DIFM) subsystem capable of determining the frequency of unknown signals over a 500-MHz bandwidth, centered on 4 GHz, with a resolution of ±7.8 MHz. The system consists of three parts: a limiting amplifier and filter, a comparator and data processing unit operating at room temperature, and a cryogenic subsystem containing five discriminator modules based on superconductive delay lines, GaAs mixers and power dividers. With a single-tone CW input between −40 dBm and +10 dBm, the frequency quantization boundaries of the subsystem are, on average, 3.1 MHz from their design values. This system was built for the High-Temperature Superconductor Space Experiment, Phase II (HTSSE II). It has passed all required qualification tests for vibration, shock and thermal cycling. The system is currently scheduled for satellite launch in fall 1996. Compared to a conventional system, the superconductive version of the DIFM is considerably smaller and provides enhanced resolution. In addition, the technology employed can be readily extended to a system with additional bits and wider instantaneous bandwidth. The system built demonstrates the potential for system-level applications of high-temperature superconductive electronics in instrumentation, communications, radar, and electronic warfare.**

I. Introduction

THE inherent low surface resistance of superconducting materials makes possible microwave devices and circuits with very high Q, low insertion loss and low dispersion. The discovery of high-temperature superconductors (HTS) has fundamentally changed the prospects for applications of superconductive components in electronic systems. A variety of devices based upon HTS technology—including resonators, delay lines, filters, couplers, and antennas—have already been demonstrated. In this paper, we present the results obtained from a digital IFM subsystem, which is one of the first demonstrations of HTS electronics at the subsystem level.

Instantaneous frequency-measurement (IFM) subsystems are widely used in electronic-warfare (EW) and electronic-intelligence (ELINT) systems for determining the frequency of unknown signals over a broad frequency band [1]. They perform this function by comparing the phase of an unknown signal with the phase of a time delayed replica of the same signal. In order to perform this function accurately, wideband long microwave delay lines are utilized. The accuracy of the reported frequency in DIFM systems is largely dependent on the length and fidelity (i.e., phase accuracy) of these delay lines.

For communication and surveillance applications, scanning superheterodyne receivers have the advantage that they can distinguish simultaneous emitters and can extract data from a given carrier. However, scanning receivers have a limited instantaneous bandwidth or, equivalently, a small probability of intercept (POI). An IFM, on the other hand, is sensitive at all times to its entire bandwidth and can be used to cue a scanning receiver to the frequency of a detected emitter.

Channelized receivers, consisting of a bank of narrowband filters with contiguous bands, have a higher POI than scanning receivers because of their high degree of parallelism. This parallelism, however, comes at the price of increased size, weight and possibly power. Practical considerations make it difficult to cover wide bands with high POI. The use of an IFM to cue the filter bank to bands with activity can significantly enhance system effectiveness.

The chirp-transform spectrum analyzer is also a widely used system. It offers both wide bandwidth and high POI. Chirp-transform systems are, however, much more difficult to implement, requiring precisely tapped delay lines (rather than the untapped delay lines used in DIFM), mixers with wide dynamic range, circuits to detect pulses as short as the reciprocal of the system bandwidth and fast gating circuitry. A superconductive chirp-transform spectrum analyzers have previously been demonstrated [2]. DIFM's, by contrast, have moderately high sensitivity, high dynamic range, excellent frequency accuracy, high POI and broad instantaneous bandwidth [3] and [4].

Conventional DIFM systems use delay lines made by coiling coaxial cables or (for shorter delays) by patterning meander lines of normal-metal microstrip. However, the loss and bulk associated with these approaches limit the amount of available delay. In order to recover sufficient frequency resolution with short delay lines, system designers are forced to use precision phase detection schemes, placing stringent demands on the mixers, phase shifters, and baseband circuitry used in the phase detectors [5]. Superconductive delay lines offer higher bandwidth combined with the lowest loss and dispersion compared to any other currently available technology. Long, low-loss, broadband superconductive delay lines can enable the use of

Manuscript received November 14, 1995; revised February 15, 1996. This work was sponsored by the U.S. Naval Research Laboratory

The authors are with Conductus, Inc., Sunnyvale, CA 94086 USA.

Publisher Item Identifier S 0018-9480(96)04804-1.

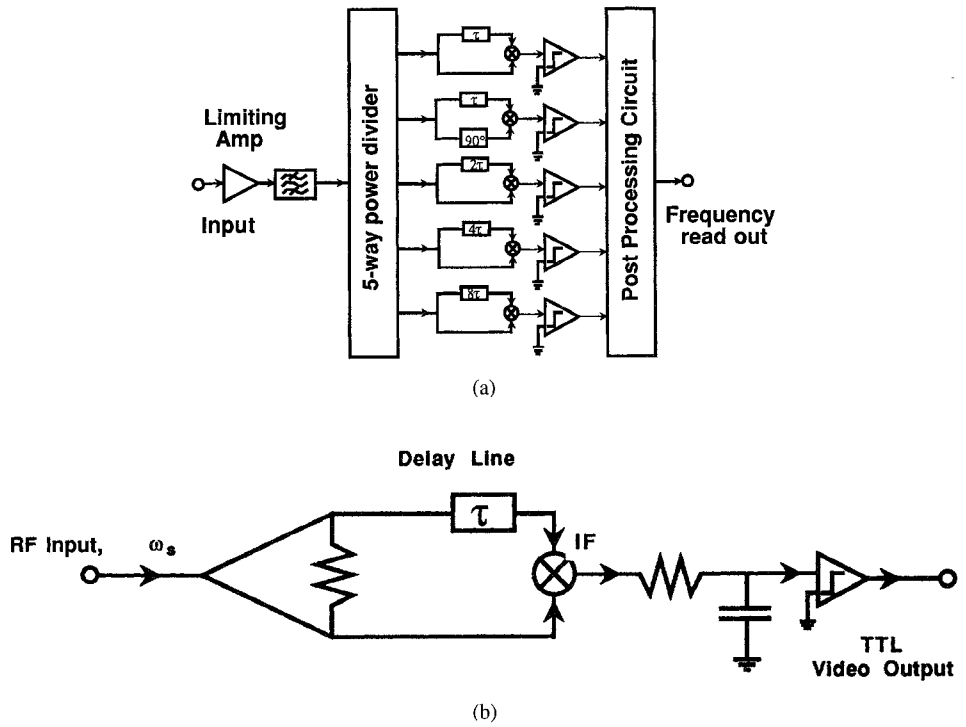

Fig. 1. (a) Schematic diagram of the DIFM subsystem. (b) Schematic diagram of the DIFM phase discriminator.

simple binary phase detection for frequency determination. One intrinsic limitation of IFM systems is that only one tone can be measured at a given instant, and other spectral components may degrade the measurement.

II. Architecture of the DIFM Subsystem

The architecture of the present DIFM subsystem is shown in Fig. 1(a) [6]. The incoming IF signal is split by a five-way power divider to feed five phase-discrimination channels, each of which provides one bit of the output frequency word. In each channel, the power is further split into two paths, one of which is applied directly to the LO port of the correlation mixer while the other is routed through a delay line, the output of which is fed to the mixer RF port. In traversing the delay line, the signal will experience a phase shift, with respect to the undelayed signal, which is a function of the input frequency. The phase correlation is obtained by lowpass filtering the output of the mixer. This baseband output is then hard-limited to obtain the appropriate bit of the binary representation of the input signal frequency.

The delay in successive channels of the DIFM is incremented by factors of two, with the exception of the two most significant bits (MSB's), which are the same length but are 90° out of phase. This configuration produces a Gray code, which is then converted to natural binary code, and then to decimal form. The processing time needed to accomplish this measurement, and hence the minimum length pulses which can be processed, is on the order of the time delay of the least significant bit (LSB) discriminator. The time delay associated with the LSB discriminator of a DIFM that uses a set of basic cosine binary correlators is given by $\tau_d = 1/(4f_r)$, where f_r is the desired frequency resolution.

The key elements in the subsystem are the delay lines and the phase comparators. The resolution of the frequency determination is dependent on the length of the delay line; it is given by $\pm(8\tau_{\max})^{-1}$ where $\tau_{\max}$ is the length of the longest delay. In our subsystem, the longest line is 16 ns, giving a resolution of ± 7.8 MHz. (Resolution may also be enhanced by performing multi-bit phase measurements on the output of the branch with the longest delay). It is very important that deviations from linear phase (constant group delay) be minimized in these delay lines, as such deviations result directly in errors in the frequencies at which the output bits switch. It is also critical that the line lengths be accurately controlled.

As shown in Fig. 1(a), a DIFM subsystem uses a bank of frequency discriminators with the longest delay corresponding to the desired frequency resolution, while the shortest delay is determined by the bandwidth to be measured. The discriminator of the DIFM receiver shown in Fig. 1(b) provides IF voltages proportional to $\cos \omega_s \tau_d$. Processing $\cos \omega_s \tau_d$ through a binary comparator produces an output with transitions at angular frequencies $\omega_n = (n+1/2)\pi/\tau_d$. A set of m comparators with binary outputs can divide the unambiguous frequency range corresponding to the shortest-delay correlator into 2^m frequency cells. In our design, we chose the frequency range of 3.75–4.25 GHz. We used 5 delay lines having delays of 16 ns, 8 ns, 4 ns, 2 ns, and 2 ns, respectively. Fig. 2 shows the ideal output waveforms of that system. It is clear from Fig. 2 that the performance of the system is fully characterized by the ω_n at which the transitions between frequency bins occur. As stated above, these transition frequencies should be at $f_n = (n + 1/2)/2\tau_d$. The deviations of the measured transition frequencies from this design value are an important performance measure.

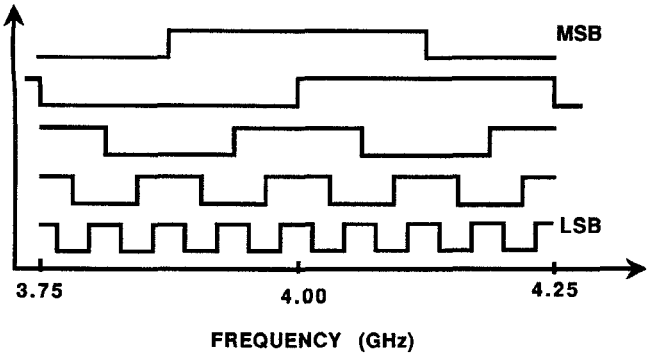

Fig. 2. Ideal DIFM digital output waveforms. 2-ns (in phase), 2-ns (quadrature), 4-ns, 8-ns, and 16-ns channels are arranged from the top to bottom.

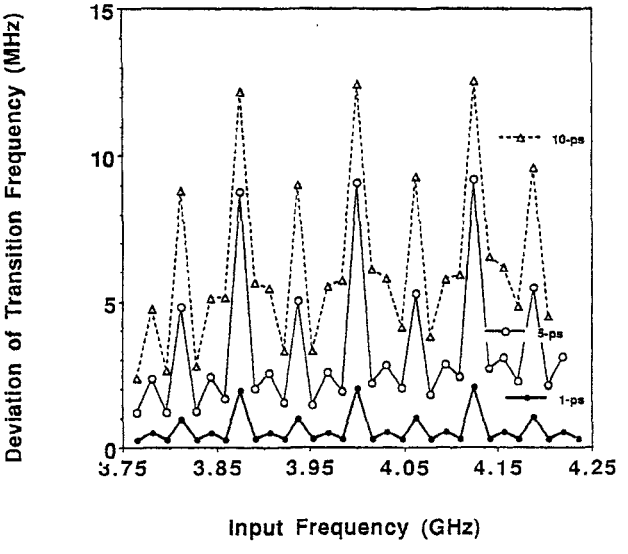

Fig. 3. Standard deviation of the transition frequency error versus design frequency calculated from assumed delay-line length variations. Each delay line is assumed to have an independent Gaussian distributed delay error about its nominal delay value with a deviation of 1 ps (bottom curve), 5 ps (middle curve), and 10 ps (top curve).

Fig. 3 shows the predicted standard deviation of the transition frequency as a function of input frequency, if there were variations in delay line length. The amount of delay of all five delay lines have Gaussian distribution errors about their nominal design values with standard deviations of 1, 5, and 10 ps. In the simulation, the quantization error is not included. As we can see, the deviations due to shorter delay lines create larger deviations in transition frequencies and the deviations of the transition frequencies due to a particular delay line increase with the input frequency. As expected, larger errors in delay line lengths cause larger errors in transition frequencies. The requirement on the precision of the delay line length will become tighter if the quantization is made smaller (i.e., longer delay lines are used).

An important issue associated with the discriminator is establishing an accurate zero reference to ensure that switching occurs at the designed frequency value. Otherwise, errors in the reported frequency occur. This possible offset could be caused by imbalance and phase errors in the RF circuitry and the lack of matching of diode characteristics. A performance analysis has been done for variations in the zero reference of the comparator. In the analysis, it is assumed that a limiting amplifier is used in front of the DIFM cryogenic section so that the input signal (and, in turn, the output of the mixer) are of constant magnitude. If there is no error, the frequency readout will represent no more than the quantization error. But if there is a Gaussian distribution zero reference error in the five channels with an rms value of 10% of the mixer output magnitude, frequency readout error will be slightly more severe than the quantization error. Finer quantization, of course, will tighten this rather loose requirement.

III. Implementation of the DIFM

The system utilizes HTS materials extensively. The delay lines are made from $YBa_2Cu_3O_{7-\delta}$ (YBCO) on 20-mil-thick $LaAlO_3$ substrates in a stripline configuration. The other circuits are made on M-plane sapphire substrates in a microstrip configuration. We have used modified Wilkinson power dividers to split the incoming signal into five paths. The phase-detection mixers use GaAs diodes. To reduce the operational power level and thermal load, we use low-barrier-height Schottky diodes as mixing diodes at 77 K. We utilized silicon comparators and encoders for post processing. Key components are discussed further below.

A. Limiting Amplifier

The limiting amplifier, with a bandpass filter, is used to increase sensitivity and clean up the signal within the band of interest. The limiting amplifier has the advantage of reducing the discriminator output sensitivity to variations in the signal level, thus improving frequency accuracy. The limiting process also reduces the effects of simultaneous input tones because of the well-known small-signal-suppression effect of limiters. The sensitivity of an IFM receiver with a limiting amplifier is primarily determined by the noise figure of the limiting amplifier.

We have used a five-stage GaAsFET amplifier which has an input power range from -40 dBm to $+10$ dBm and output power of 16 dBm. With the output filter, the suppression of adjacent harmonics is over 35 dB.

B. Delay Lines

The bandwidth, resolution, accuracy, and sensitivity of the IFM subsystem is largely determined by the length and the quality of the delay lines. Delay lines are also useful devices for signal storage and processing. Common devices of this type include normal-metal electromagnetic delay lines, surface acoustic wave (SAW) devices, and bulk ultrasonic delay lines. Compared to these delay lines, superconducting delay lines offer the highest bandwidth with the lowest loss and dispersion. In fact, superconducting thin films are the only technology capable of achieving long delays of high-frequency signals with low losses in highly compact designs.

Several planar transmission line structures can be used to make delay lines. Striplines are particularly suitable for delay-line applications at microwave frequencies, offering

nearly pure TEM propagation, a densely packaged structure, insignificant radiation loss and minimized current crowding at the edges of the line. We have made delay lines on different substrates ($LaAlO_3$ and sapphire) with different thicknesses (five-mil-thick to 20-mil-thick). We have successfully fabricated a 44 ns delay line on a single 2-in wafer. The key issues in delay-line design include obtaining the desired impedance, maximizing line-to-line decoupling, minimizing the air gap between wafers and making a reflection-free transition from the stripline circuit to the other circuit elements or to SMA or other connectors. Phase noise, or specifically, phase linearity, is very important especially if the delay line is to be used for phase measurements or more sensitive frequency measurements.

In the IFM system, all the delay lines were made using YBCO films on 20-mil-thick $LaAlO_3$ substrates using a dual-spiral geometry [7]–[9]. The linewidth of all five delay lines was 100 μm (with 45-Ω characteristic impedance) with tapered-line transformers at both ends [9]. The characteristic impedance at the beginning and the end of the line was 50 Ω.

A stripline requires that the substrates be held in intimate contact with each other as the device is repeatedly cycled between room temperature and cryogenic temperatures. To insure phase reproducibility in a delay line structure that stores many wavelengths of analog signal, the residual air gap between the two substrates must be less than a fraction of a micron; otherwise, the change of impedance will cause severe reflection and generate microphonics due to mechanical vibration. Fig. 4(a) shows the mechanical package for the delay line. It contains a base plate, spacers, a spring retainer and a top cover. The ground plane contact is made with silver foil between the ground plane of the top wafer to the package. Additional silver foil is placed below the bottom wafer to make a good contact. We have used a bed of beryllium-copper (BeCu) springs to press against the thin dielectric substrates and keep them in intimate contact with each other [10] and [11]. Fig. 4(b) shows the stripline delay line layout for a 44 ns delay line.

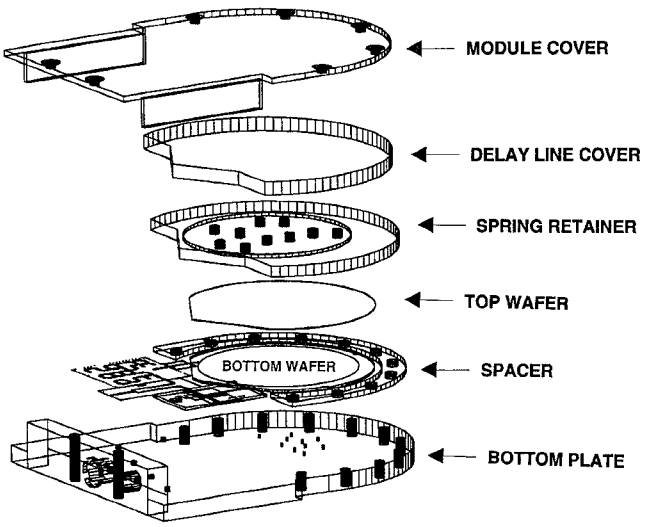

(a)

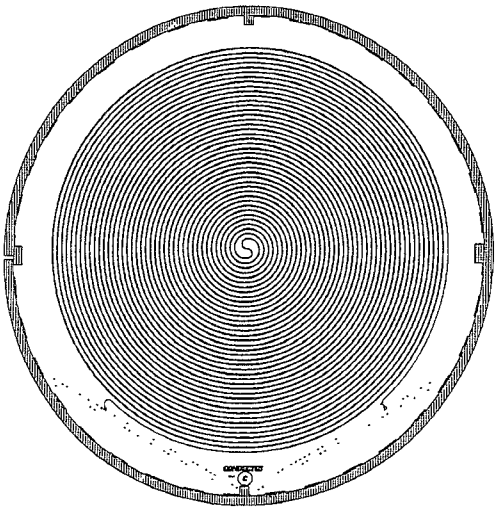

(b)

Fig. 4 (a) Diagram of delay line package. (b) Layout of stripline delay line on a five-cm-diameter $LaAlO_3$ wafer.

C. Cryogenic Mixers

Phase-detecting mixers serve as part of phase discriminators. Three common types of mixers include single-ended, single-balanced, and double-balanced. For our application, low power dissipation is very important. Therefore, the third approach is not very attractive because of its high power consumption. The single-ended mixer is too sensitive to its termination, has minimal tolerance to large signals and has very narrow bandwidth. It is also poor at suppressing spurious signals. Therefore, the single-balanced approach is a natural choice. For that mixer, we need either a coupler or a balun. Two separate diodes are required for the coupler approach and it is difficult to match them closely. As a result, we chose to use a balun approach with a T-type matched diode pair.

Because of power constraints and the required performance for phase detection, mixers should have low conversion loss, low noise figure, high LO/RF isolation and low LO drive power. By operating the mixers within the cryogenic enclosure, only one IF cable (with low thermal conductance) per discriminator is required, while two microwave cables (with higher thermal leakage) would be necessary if the mixers were at room temperature. At cryogenic temperatures, the I–V curve of a Schottky diode is much steeper than at ambient temperature. This steep I–V curve creates a large current swing for a given voltage change. This increased nonlinearity makes possible low-power operation with low noise and low conversion loss. However, at low temperature the barrier height is increased, in turn increasing the required LO power for self-biased operation. We use low-barrier-height diodes to reduce the operating power level. The diode we used has a barrier height of 0.2 V. This type of diode requires only 5–7 dBm LO power in a self-biased single-balanced configuration for good mixer performance at low temperature.

The measured I–V curve of a low-barrier diode at 77 K and 300 K are different [6]. As the temperature is lowered, the diode becomes more sensitive to applied voltage, with the

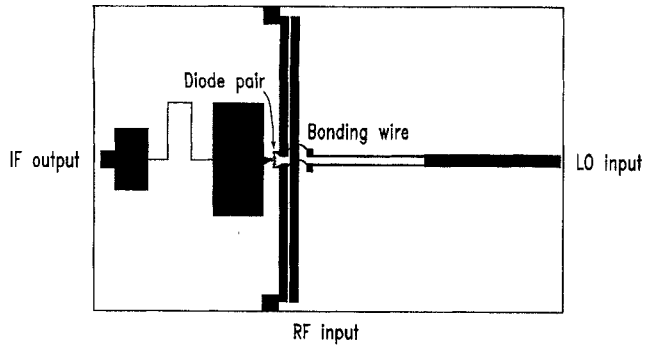

(a)

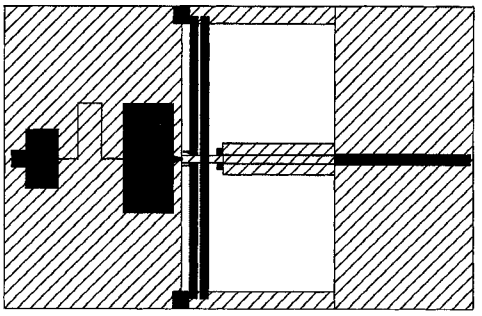

(b)

Fig. 5. (a) Layout of the mixer showing the metallization pattern. (b) Layout of a mixer with ground plane shown. The hatched area is the ground plane on the back side of the wafer. As can be seen, the ground plane is partially etched in this design.

diode knee increasing in voltage. Fig. 5(a) is the layout of the mixer which is made with silver on a 25-mil-thick sapphire substrate. As shown in the figure, the LO signal is applied to a microstrip launcher and the RF signal is coupled to the diodes by two sections of quarter-wave balun. In order to achieve the proper coupling, we etch away the ground plane of the mixer under two coplanar strip lines. Fig. 5(b) shows the layout of the mixer with the ground plane presented. The hatched line represents the ground on the backside of the wafer. The ground plane is partially etched away. In addition, there is a recess at the bottom of the package under the region where the ground plane is etched away. A low-pass filter is followed by the diode pair.

D. Power Divider

There are two types of power dividers used in this system. One is a five-way power divider feeding the discriminators and the others are the two-way power dividers within each discriminator. Both of them are made with silver on sapphire substrates. We utilize a standard Wilkinson power divider for two-way splitting with thin-film resistors. For the five-way power divider, we have modified a conventional power divider. The power dividers commonly used are the Wilkinson, radial and planar structure [12]–[16]. The Wilkinson type has the advantages of being low-loss and having moderate bandwidth with good amplitude and phase balance. However, its major disadvantage is its nonplanar crossover configuration. The radial-line divider has low loss, inherent phase symmetry and

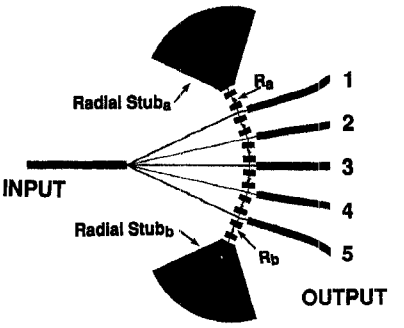

Fig. 6. Layout of a five-way power divider.

good isolation, but it requires a three-dimensional structure [14]. The planar N-way combiner [15] requires $(N-1) \times N$ quarter-wave sections for maximum isolation and thus is very large in size. It also suffers from isolation, return loss and output power variation.

In order to make a power divider which has low loss, broad bandwidth and good symmetry in a planar structure, we modified a planar power divider structure. It has the combined advantages of the planar N-way combiner and the radial structure. Fig. 6 shows the layout of our power divider. We have added two radial stubs and two resistors R_a and R_b for more symmetry, to increase the bandwidth and to enhance the isolation. The high-impedance stub lines between resistors increase the isolation of the output channels. Calculations predict that the return loss of the input and all outputs are more than 20 dB, and the isolation is over 20 dB. The output power split is designed to be unequal to compensate for the insertion-loss differences in the different delay lines. At 4 GHz, the design output powers in this divider are -6.5 dB (port 3), -7.0 dB (ports 2 and 4), and -9.5 dB (ports 1 and 5).

One of MSB channels requires a quadrature phase shift. We use a four-finger interdigital coupler (Lange coupler with four 48-μm-wide fingers). In this structure the crossovers are implemented by wire bonding.

E. Room-Temperature Post-Processor

The comparator output is designed to be five-bit Gray code, representing the instantaneous frequency of the input signal. The Gray code is converted to binary code and then to decimal and finally is displayed. Specifically, the room-temperature post-processor consists of three parts: one is the comparator, the second is the Gray code-to-BCD convertor and the third is an LED display driver. The comparators are the LM161/361 high speed differential type. They give a square-wave output of up to 30 MHz. The GAL20V8A is used to do the Gray-to-BCD conversion; it is also clocked with a 10 KHz signal to provide a proper output to the display driver. The maximum clock frequency is 33 MHz. We use a PAL20RP8 as a display driver. The materials used were carefully chosen to meet all space application requirements. The package is carefully designed and extensively analyzed to pass vibration tests. We performed a simple mechanical calculation to determine the static mechanical response, i.e., the first natural frequency, and

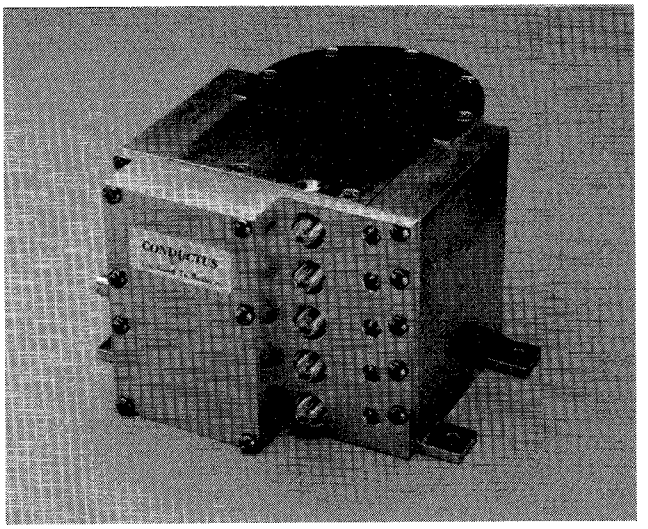

(a)

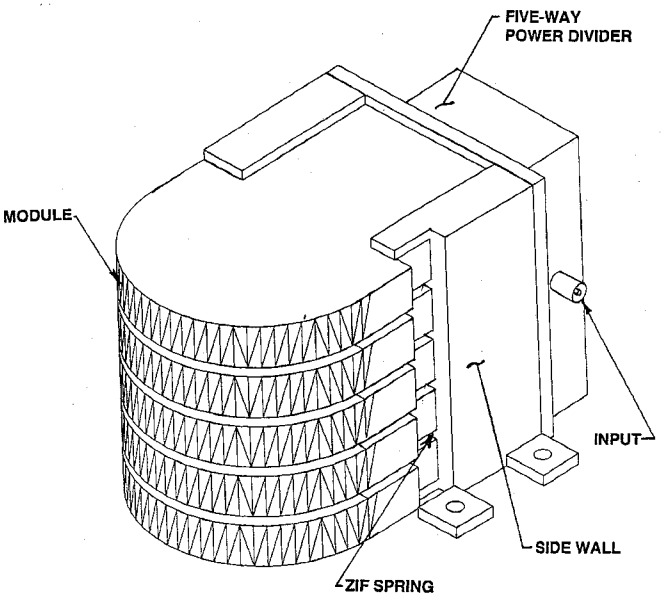

(b)

Fig. 7. (a) Cryogenic section of flight DIFM system. The front left section is the five-way power divider. As can be seen, the input is feed through the SMA connector, then through the five-way power divider, and then feeds into five different modules. The five output connectors are on the front side. (b) The schematic diagram showing the cryogenic section of the second-generation flight DIFM. There are two side walls with five extensions in inner sides to accept and support five modules, incorporating zero insertion force springs, which create good electrical, thermal, and mechanical connections among these modules.

then used finite element analysis to determines the static and dynamic mechanical responses.

F. Package for Cryogenic Section

The overall package consists of six gold-plated aluminum subpackages. Five of these are discriminator modules containing mixers and delay lines, which are a combination of stripline and microstripline configurations. The sixth subpackage contains the five-way power divider in a microstrip configuration. These six subpackages are electrically connected by five "snap on" SMA connectors. Fig. 7(a) is a photograph of the assembled cryogenic section of the DIFM system. The front-left section is the five-way power divider. As can be seen, the input is fed through the SMA connector, goes through the five-way power divider and then feeds into five different modules. The five output signals are adjacent to the five-way power divider. The reduction in size and the improved robustness compared to our previous unit [6] is clear. Fig. 7(b) is a three dimensional drawing of this cryogenic section of the second-generation flight DIFM. There are two side walls with five extensions in inner sides to accept and support five modules, incorporating zero insertion force springs, which create good electrical, thermal, and mechanical connections among these modules. Fig. 8 shows a 16-ns discriminator module. The components shown are: bottom left—trimming delay line; bottom middle-a two-way power divider; bottom right—a self—biased mixer; upper right—a spiral delay line on $LaAlO_3$ substrate, with upper ground plane of the stripline removed to reveal the pattern.

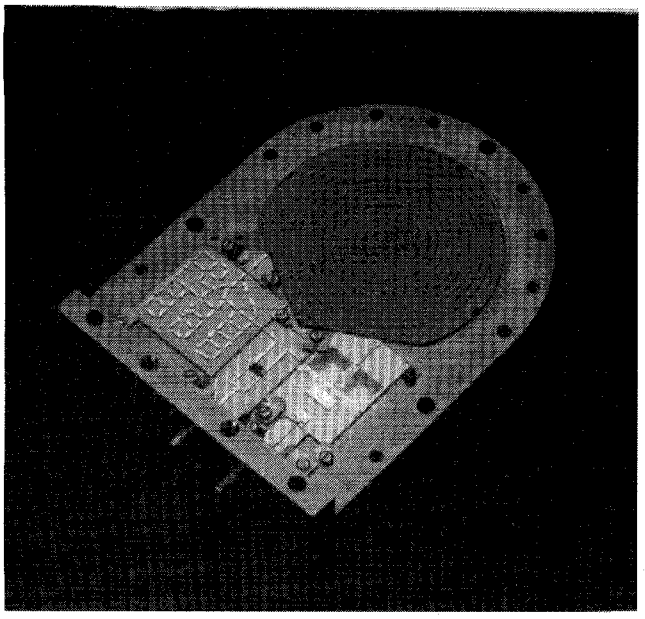

Fig. 8. Discriminator modules with 16 ns delay line. The components are: bottom left—trimming delay line; bottom middle—a two-way power divider; bottom right—a self-biased mixer; upper right—a spiral delay line on $LaAlO_3$ substrate, with upper ground plane of the stripline removed to reveal the pattern.

G. Final Fight Unit Package

We performed vibration and shock tests upon the acceptance unit we reported previously (Fig. 7 in [6]). The results of those tests were that the overall package was not rigid enough and the thermal resistance across each module was too large. Based upon these results, we made several significant changes to the package in the second iteration for the flight unit. First, we reduced the thermal mass of all components. Second, we rotated the five-way power divider in order to reduce its footprint and to improve the thermal contact. Third, we constructed a pair of side walls with five extensions on their inner sides to accept and support the five discriminator modules. This trays-in-rack structure incorporates zero insertion force (ZIF) circuit board retainers, which create good electrical, thermal and mechanical connections among the modules [17]. Unlike the unit shown in our previous work [6], all the modules in the final unit were more tightly connected (mechanically, electrically and thermally) primarily as a result of using the ZIF springs.

IV. Fabrication

YBCO films were made by the off-axis sputtering technique [18] and [19]. Patterning of the film was done by argon ion-beam etching, using standard positive photo resist. We used sputtered silver and gold for bonding pads. For the normal-metal circuits, we used sputtered silver or gold on 25-mil-thick M-plane sapphire substrates, using a molybdenum adhesive layer. Normal-metal films are also patterned by an ion-milling dry etch technique. Ground planes for the delay lines consist of either silver (for 2-, 4-, and 8-ns delay lines) or YBCO films (for the 16-ns delay line). The wire bonding was done with either an ultrasonic wire bonder or a gap welder using either five-mil-wide and 20-mil-wide ribbon.

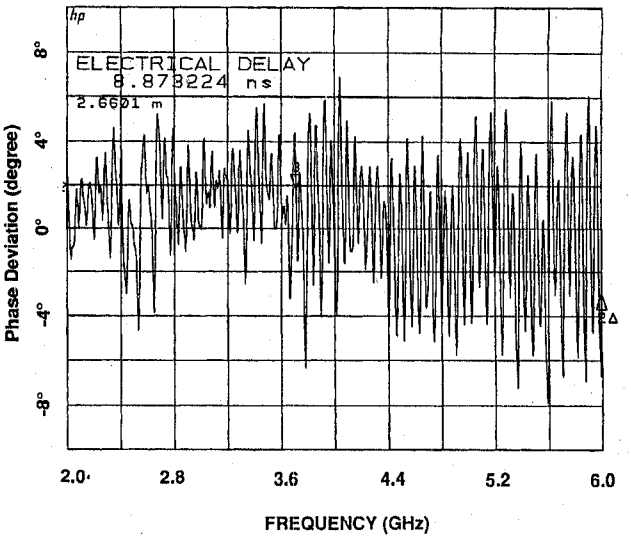

Fig. 9. Phase deviation from linear for a typical superconductive stripline delay line. A linear phase corresponding to 8.87 ns of delay has been used.

V. Experimental Results and Discussion

We have fabricated and tested each part of the subsystem and evaluated the overall system performance. The performance of the components, modules and complete IFM system is described below.

A. Delay Lines

Scattering parameters of these delay lines have been measured outside of the discriminator modules. In addition, a comparable delay line—a 15.2 ns delay line on $LaAlO_3$ made at Conductus—has less than 1-dB insertion loss at 77 K at 6 GHz. As mentioned, the phase linearity of the delay line is very important. Superconductive lines have a very small insertion loss and dispersion with the result that high-speed signals can propagate with high fidelity. Fig. 9 shows phase deviation from linearity for a typical superconductive stripline delay line. A linear phase corresponding to 8.87 ns of delay has been used. The RMS value of phase deviation is 2°.

B. Cryogenic Mixers

The conversion loss versus frequency is shown in Fig. 10. At 4 GHz this was measured to be 7 dB at 77 K and 10 dB at 300 K. The variation is ±0.75 dB within the 500-MHz bandwidth. In this measurement, both LO and RF had a power level of 7.5 dBm. The LO/RF isolation is 18–22 dB, and the LO/IF isolation is over 40 dB.

C. Power Dividers

The measured return loss for the two-way power divider is over 15 dB. The insertion loss to both output ports is 3.1±0.1 dB across the band. The five-way power divider shows a 16-dB return loss on the input port, 23- to 28-dB return loss on the outputs, and a 20–25 dB isolation between the outputs. The output power split at 300 K is −7.1 dB (port 3), −8.5 dB (ports 2 and 4), and −9.3 dB (ports 1 and 5).

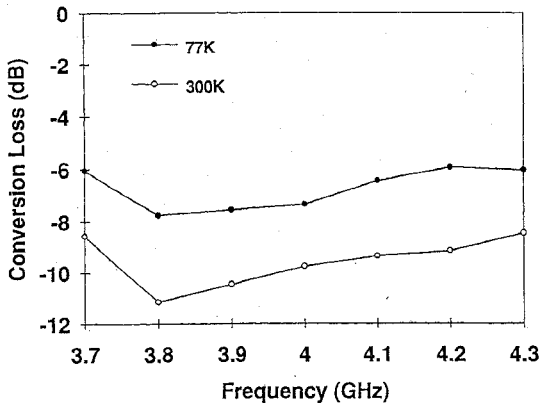

Fig. 10. Measured conversion loss of the mixer at 77 K and 300 K.

D. One-Bit Discriminator Module

A delay-trim network is used in conjunction with the delay line as shown in Fig. 8. Alternate paths through the Au/sapphire microstrip trim circuit are selected by wire bonding so that the zero crossings of discriminator IF outputs occur at the design frequencies. The delay can be trimmed in units of 36 ps, and fine trimming can be made to 10 ps. Each comparator threshold value is also independently adjusted. The cryogenic section is initially tuned in LN_2. Because of the nonunity dielectric constant of LN_2, the frequency response of the device will be different if it is operated under vacuum. We developed a simple testing setup where one can test the device in N_2 gas at 77 K. All the units were tested in this test setup before we tested them in a cryostat.

A superconductor has a penetration depth for magnetic fields that is analogous to the skin depth in normal metal. While this penetration depth is not a function of frequency, it is temperature- dependent, particularly for temperatures close to the superconducting critical temperature. As the temperature decreases, the penetration depth is reduced. This will reduce the kinetic inductance, and, in turn, the amount of delay created [20] in a superconductive delay line. The DIFM modules are stable at temperatures below 72 K and show an approximately 6 MHz effective drift between 72 and 77 K. Fig. 11 shows the IF output of a 16 ns discriminator versus operating temperature. The central 100 MHz of bandwidth is shown on an expanded scale. As one can see, the response differs as a result of kinetic inductance changes with temperature.

E. Complete System Test

The complete system was first tested in liquid nitrogen and then tested in a cryostat. Fig. 12 shows the output of the post-processor unit, with a single swept input tone, as a function of the input frequency. The outputs of the 2-ns (in phase), 2-ns (quadrature), 4-ns, 8-ns, and 16-ns channels are arranged from top to bottom. Fig. 13 shows the digital output of the room- temperature post-processor corresponding to Fig. 12. Fig. 14 shows the frequency reported by the DIFM, under CW conditions with a single stepped input tone, where the x-axis is the input frequency and the y-axis is the readout frequency indicated by the decoded binary signals shown in Fig. 13. The

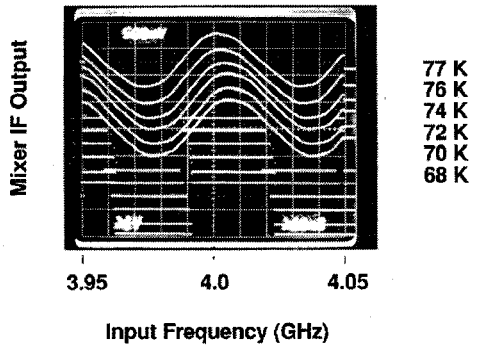

Fig. 11. IF output of a 16 ns discriminator versus operating temperature. The central 100 MHz of bandwidth is shown on an expanded scale.

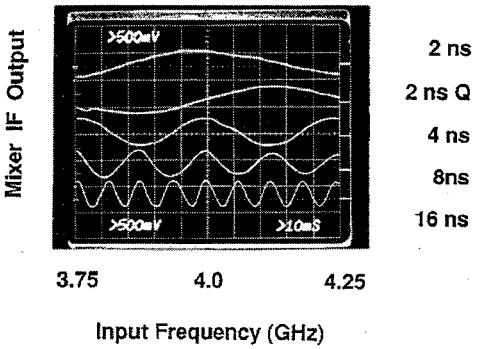

Fig. 12. The five-bit analog output of the DIFM as a function of input frequency. The curves from top to bottom represent the output of 2-ns (in phase), 2-ns (quadrature), 4-ns, 8-ns, and 16-ns channels.

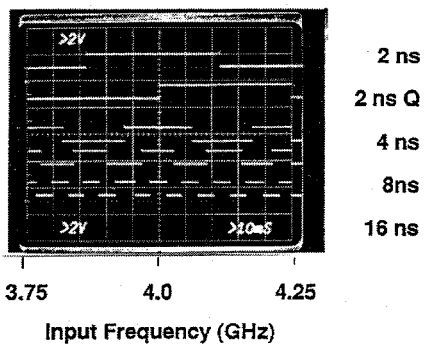

Fig. 13. The five-bit digital output of the DIFM as a function of input frequency.

average of the magnitude of the deviation of the transition frequencies (that is, the frequencies at which the binary output changes) from the design values is 3.1 MHz. Fig. 15 shows the deviation of the transition frequency from its ideal value. The input power dynamic range is between -40 dBm and $+10$ dBm. We have performed a dual-tone test without the limiting amplifier using two CW sources within the DIFM band. One source, with a constant power of 11.7 dBm, was swept over the band, while the other, weaker tone was tuned to 3.8 GHz. Fig. 16 shows the 16 ns discriminator output with two signals present with the weak signal at various power level. The DIFM accurately reports the frequency of the stronger signals as long as the weaker single is 10 dB lower. The tolerable power difference can be 6 dB smaller by use of a limiting amplifier

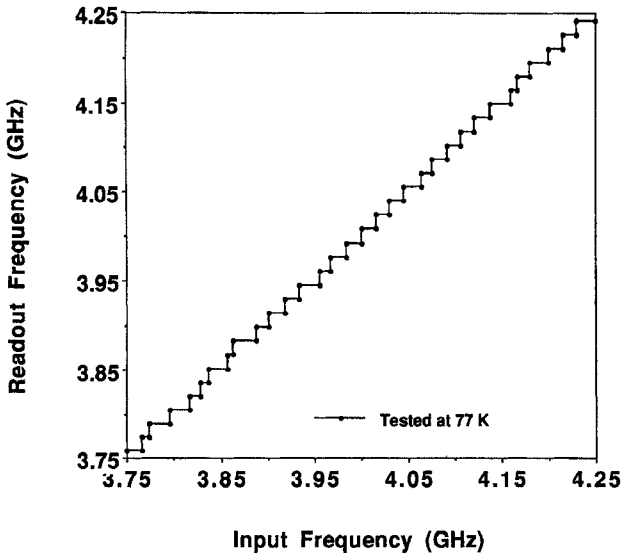

Fig. 14. DIFM frequency readout versus input frequency (CW test).

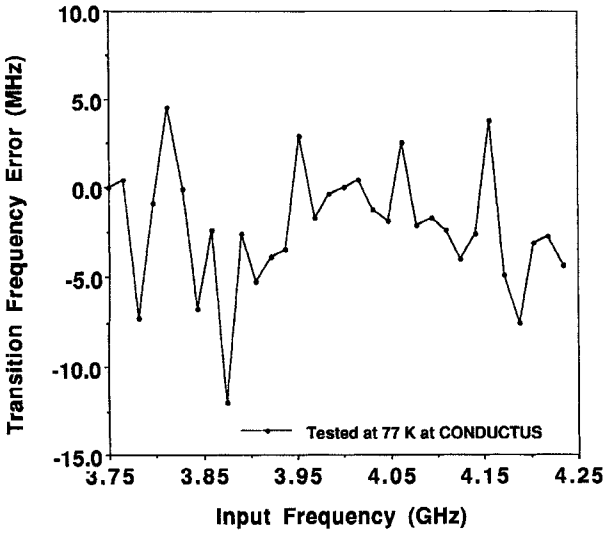

Fig. 15. Deviation of the transition frequency from ideal value.

because of its small-signal suppression effect. This effect can be enhanced if additional limiting amplifiers are used.

F. Space Qualification Test

The space qualification test was a major hurdle for the project. In order to meet this requirement, the materials selected had to meet space application specifications including electrical, mechanical, thermal and outgassing specifications. We have performed random vibration tests, shock tests and thermal cycle tests upon all parts. Each module and the integrated unit was tested. Fig. 17 shows the digital output of the system before and after the vibration test under the same measurement conditions. The solid and dashed lines represent the data before and after the vibration test. As can be seen, the deviation is very small. The cryogenic unit and room temperature unit have different vibration level requirements. In addition, the vibration level is different depending on the orientation of the unit with respect to the mounting plate

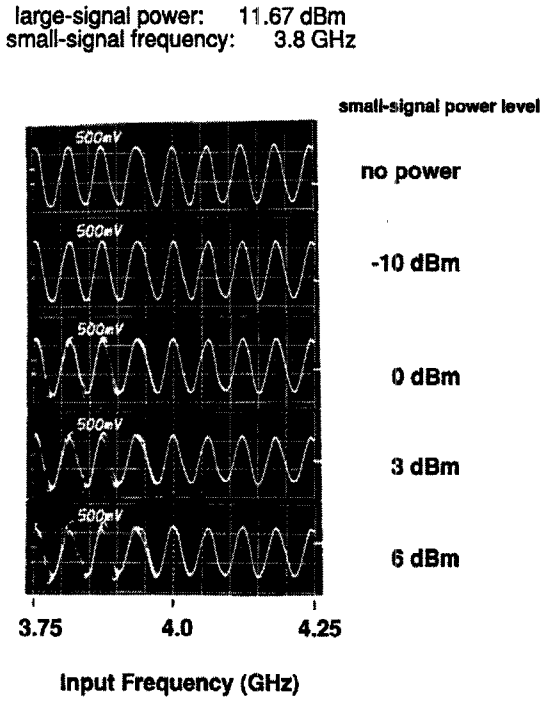

Fig. 16. IF output of a 16-ns discriminator, when two sources are applied at the same time. One is with a constant power of 11.7 dBm, sweeping over the band, while the other is tuned to 3.8 GHz and is of variable power. No limiting amplifier is used in testing.

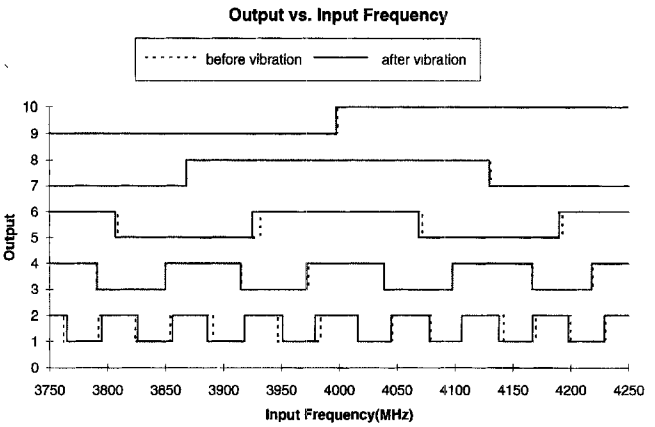

Fig. 17. Digital output of the flight unit before and after the vibration test.

direction. For the thermal test, the temperature range was between −10 to 50°C; six cycles were tested with 2 h dwell time at two extreme temperatures and a ramp rate of 1°C/min. The system had been integrated in the satellite payload. Fig. 18 is the photograph of the DIFM subsystem mounted in the satellite payload.

VI. Conclusion

We have reported a five-bit superconductive digital instantaneous frequency measurement (DIFM) subsystem. The system has a center frequency of 4 GHz and a bandwidth of 500 MHz. The subsystem contains a cryogenic section with five discriminator modules utilizing superconductive delay lines, GaAs mixers, and power dividers. The subsystem also has a

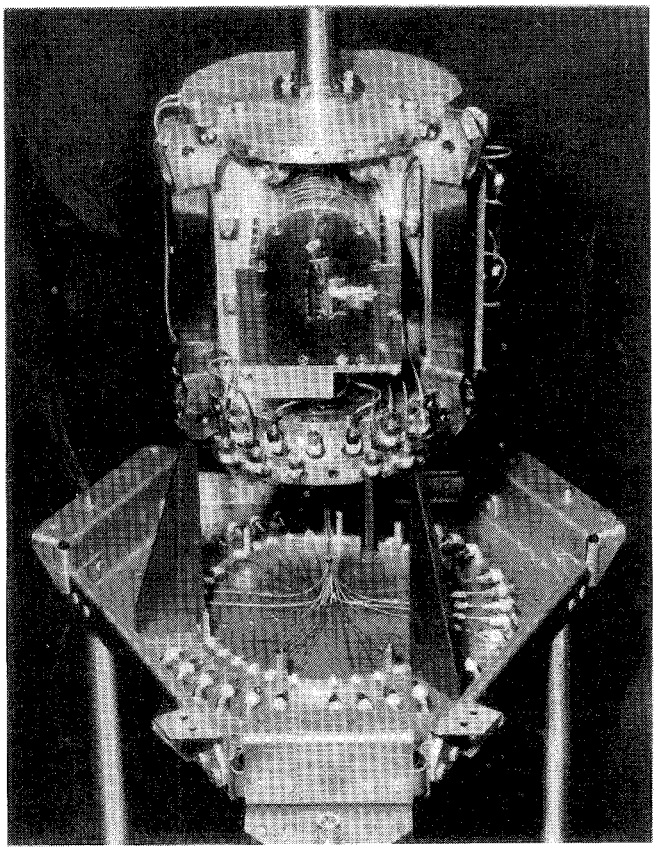

Fig. 18. DIFM subsystem mounted in satellite payload (the integration is done at NRL and this photo is taken at NRL).

room-temperature GaAs limiting amplifier and a silicon post-processor. With a single-tone CW input power between −40 dBm and +10 dBm, the frequency quantization boundaries of the subsystem are, on average, 3.1 MHz from their design values. The system has passed all its space qualification tests and, as of this writing, has been installed in a satellite payload. It is currently scheduled to launch in fall 1996.

ACKNOWLEDGMENT

The authors wish to acknowledge M. Krivoruchko, A. Barfknecht, D. Zhang, W. Ruby, and J. Ramsden at Conductus for their assistance and consultation. Special thanks to M. Nisenoff, T. Kawecki, S. Chappie, J. Pond, and H. Newman at Naval Research Laboratory for help with various issues.

REFERENCES

[1] J. B.-Y. Tsui, *Microwave Receivers with Electronic Warfare Applications,* New York: Wiley, 1986.

[2] T. C. L. G. Sollner, W. G. Lyons, D. R. Arsenault, A. C. Anderson, M. M. Seaver, R. R. Boisvert, and R. L. Slattery, "Superconducting cueing receiver for space experiment," *IEEE Trans. Appl. Superconduct.,* vol. 5, pp. 2071–2074, June 1995.

[3] J. B.-Y. Tsui, *Microwave Receivers and Related Components,* Avionics Laboratory, Air Force Wright Aeronautical Labs., 1983.

[4] E. Wolff and R. Kaul, *Microwave Engineering and Systems Application.* New York: Wiley, 1988.

[5] R. Bauman, "Digital instantaneous frequency measurement for EW receivers," *Microwave J.,* p. 147, Feb. 1985.

[6] G.-C. Liang, C. Shih, R. S. Withers, B. Cole, M. E. Johansson, and L. P. Suppan, "Superconductive digital instantaneous frequency measurement subsystem," *IEEE Trans. Microwave Theory Tech.,* vol. 41, pp. 2368–2374, Dec. 1993.

[7] G.-C. Liang, R. S. Withers, B. F. Cole, and N. Newman, "High-temperature superconductive devices on sapphire," *IEEE Trans. Microwave Theory Tech.,* vol. 42, Jan. 1993.

[8] W. G. Lyons, R. S. Withers, J. M. Hamm, A. C. Anderson, P. M. Mankiewich, M. L. O'Malley, and R. E. Howard, "High-Tc superconductive delay line structures and signal conditioning networks," *IEEE Trans. Magnetics,* vol. 27, pp. 2932–2935, Mar. 1991.

[9] R. W. Klopfenstein, "A transmission line taper of improved design," in *Proc. IRE,* pp. 31–35, 1956.

[10] A. C. Anderson, R. S. Withers, S. A. Reible, and R. W. Ralston, "Substrates for superconductive analog signal processing devices," *IEEE Trans. Magn.,* vol. 19, pp. 485–489, May 1983.

[11] G. C. Liang, R. S. Withers, B. Cole, S. Garrison, M. Johansson, W. Ruby, and W. G. Lyons, "High temperature superconducting delay lines and filters on sapphire and thinned $LaAlO_3$ substrates," *IEEE Trans. Applied Superconduct.,* vol. 3, pp. 3037–3042, Sept. 1993.

[12] E. Wilkinson, "An n-way hybrid power divider," *IRE Trans. Microwave Theory Tech.,* vol. 8, pp. 116–118, Jan. 1960.

[13] W. Yau and J. M. Schellenberg, "An n-way broadband planar power combiner/divider," *Microwave J.,* vol. 29, pp. 147–151, Nov. 1986.

[14] J. M. Schellenberg and M. Cohn, "A wideband radial power combiner for FET amplifier," *IEEE Int. Solid State Circuits Conf. Digest,* pp. 164–168, Feb. 1978.

[15] A. A. M. Saleh, "Planar electrically symmetric n-way hybrid power divider/combiners," *IEEE Trans. Microwave Theory Tech.,* vol. 28, pp. 555–563, June 1984.

[16] N. Nagai, E. Mackawa, and K. Ono, "New n-way hybrid power dividers," *IEEE Trans. Microwave Theory Tech.,* vol. 25, pp. 1008–1012, Dec. 1977.

[17] Private communication with T. Kawecki and S. Chappie, Naval Research Lab.

[18] N. Newman, K. Char, S. M. Garrison, R. W. Barton, R. C. Taber, C. B. Eom, T. H. Geballe, and B. Wilkens, "$YBa_2Cu_3O_{7-d}$ superconducting films with low microwave surface resistance over large areas," *Appl. Phys. Lett.,* vol. 57, pp. 520–522, May 1990.

[19] B. F. Cole, G.-C. Liang, K. Char, G. Zaharchuk, and J. S. Martens, "Large-area YBCO films on sapphire for microwave applications," *Appl. Phys. Lett.,* vol. 61, pp. 1727–1729, Oct. 1992.

[20] T. Van Duzer and C. W. Turner, *Principles of Superconductive Devices and Circuits.* New York: Elsevier, 1981.

Guo-Chun Liang (S'87–M'90–SM'94) received the B.S. degree from the East China Institute of Technology, Naijing, China, in 1982, the M.S. degree from the University of Electronics Science and Technology of China (UEST), Chengdu, China, 1985, and the Ph.D. degree from University of California, Berkeley, in 1990, all in electrical engineering.

He worked at the microwave center of UEST in 1985 and 1986. He developed a series of RF and microwave devices, including low noise amplifiers high power amplifiers, cellular phone package and antenna, attenuators, oscillators, phase shifters, and filters. He also has done a variety of time domain numerical analyzes and simulations of rf and microwave devices such as transmission lines, amplifiers, antennas, and semiconductor and superconductor devices. He has been with Conductus, Inc., Sunnyvale, CA, since 1990, developing superconductive rf and microwave circuits and systems, including resonators, filters, mixers, delay lines, and magnetic resonance coils. He led the development of space qualified instantaneous frequency-measurements system for the Navy's High-Temperature Superconductor Space Experiment program (II). He is coordinating Conductus's effort in Consortium for Superconducting Electronics activities, collaborating with MIT Lincoln Laboratory, AT&T, and CIT on high-temperature superconductor wireless product. Currently, he is a manager in wireless technology leading the development of superconductive circuits and subsystems and cryogenically cooled electronics for wireless communication applications. His interests include rf and microwave applications of superconductivity, microwave circuits and systems, cellular phone applications, numerical analysis and simulation of practical electromagnetic problems.

Chien-Fu Shih received the B.S. degree in physics from Fu-Jen University, Taiwan, in 1969, the M.S. degree in physics from University of Wisconsin, Superior, in 1972, and the M.S.E.E. degree from Oregon State University, Corvallis, in 1978.

From 1978 to 1981, he was with Eaton Corporation as a Microwave Engineer, developing voltage controlled oscillators and multipliers. Later, he worked as an integration Engineer at Ford Aerospace Corporation, designing the transponder circuits. In 1984, he joined Hewlett-Packard Company as an Electrical Engineer designing at Tracking Generator. In 1992, he joined Conductus, Inc., Sunnyvale, CA, where he has been involved in the design and measurement of superconductive microwave subsystems, resonators, and filters.

Richard S. Withers (M'78) received the S.B. and S.M. degrees in 1976, and the Sc.D. degree in 1978, all in electrical engineering, from the Massachusetts Institute of Technology, Cambridge.

In July, 1991, he joined Conductus, Inc., Sunnyvale, CA, where he is the Manager of Magnetic Resonance and RF Technology, from the MIT Lincoln Laboratory, where he was Associate Leader of the Analog Device Technology Group. In that capacity, he co-directed Lincoln's development of microwave circuits using high-temperature superconductors. Previously, as a member of the technical staff at Lincoln from 1978 to 1984, he developed niobium tapped delay lines, silicon charge-coupled devices, and surface-acoustic-wave devices. He was the program manager for microwave networks within the Consortium for Superconducting Electronics until October 1992, and in that capacity coordinated efforts at Conductus, Lincoln Laboratory, IBM, AT&T Bell Laboratory, MIT, Cornell University, and Boston University. His interests are in the microwave and RF applications of superconductivity in such fields as communications, RF instrumentation, and magnetic-resonance instruments.

Dr. Withers is active in the microwave and RF superconductivity community. He served on the advisory panel of the High-Temperature Superconductivity Assessment of the Office of Technology Assessment of the U.S. Congress and briefed the Defense Science Board Task Force on Military System Applications of Superconductors. He has given short courses on RF applications of superconductivity for audiences at the Nordic Symposium on Superconductivity and the 1991 SPIE Conference on superconductive electronics. He co-chaired, with Robert B. Hammond, the SPIE Conference on High-T_c Microwave Superconductors and Applications in Jan. 1994.

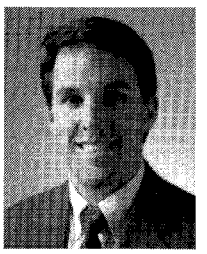

Brady F. Cole received the B.S. degree in ceramic science and engineering from The Pennsylvania State University, University Park, in 1988.

Since joining Conductus, Inc., Sunnyvale, CA, in 1989, he has investigated the growth of high-T_c Superconducting thin films. He has developed methods of depositing high quality films on large area sapphire substrates, and has established large-scale production of films with low-microwave surface resistance. His current professional interests include high-T_c multilayer films and microstructure-transport property relationships.

Marie E. Johansson received the B.S. degree in physics from the University of Linkoeping, Sweden, 1986.

From 1986 to 1989, she designed and produced passive microwave devices at the National Defense Research Institute, Linkoeping, Sweden. She then developed process techniques for high-T_c thin films at the National Institute of Standards and Technology, Boulder, CO. Since joining Conductus, Inc., Sunnyvale, CA, in June 1992, she has been working on the development and processing of high-T_c Superconducting microwave and digital devices.